Large electrocaloric responses in $[Bi_{1/2}(Na,K)_{1/2}]TiO_3$-based ceramics with giant electro-strains

Zhongming Fan, Xiaoming Liu and Xiaoli Tan*,¶

Department of Materials Science and Engineering, Iowa State University, Ames, IA 50011, USA

Abstract

The electrocaloric effect is investigated through indirect measurement in two lead-free $[Bi_{1/2}(Na,K)_{1/2}]TiO_3$-based ceramics that were previously reported to display giant electro-strains. In the Nb-doped ceramic, denoted as BNKT-2.5Nb, a decent temperature change of ΔT = 1.85 K and an electrocaloric responsivity of $\Delta T/\Delta E$ = 0.37 (10^{-6}KmV^{-1}) are found around room temperature (32 ^{o}C). While in the Ta-doped ceramic, BNKT-1.5Ta, a wide operation temperature range (T_{span} ~ 55 K) is observed near room temperature. Additional electrical measurements, as well as transmission electron microscopy experiments, are performed to identify the mechanisms of the electrocaloric effect in both ceramics.

Keywords: electrocaloric effect, $[Bi_{1/2}(Na,K)_{1/2}]TiO_3$-based ceramics, ergodic relaxor

---

This work was supported by the National Science Foundation (NSF) through Grant DMR-1465254.

*Member, the American Ceramic Society.

¶Author to whom correspondence should be addressed. Electronic mail: xtan@iastate.edu

I. Introduction

The electrocaloric effect (ECE) is the reversible temperature/entropy change ($\Delta T/\Delta S$) upon application or removal of electric field in a polar material under adiabatic/isothermal conditions.[1] When operated in a Carnot-like-four-step cycle, electrocaloric materials can produce efficient cooling on miniaturized devices.[2] Since the first electrocaloric material was discovered in 1930s, researchers have been searching for good ECE in ferroelectric materials in which the electric field is able to align the dipoles and decrease dipolar entropy. This entropy reduction under electric field tends to be maximized around the phase transition temperature where the ferroelectric phase (parallel dipoles) can be readily induced out of a relaxor phase[3,4] (random dipoles), a paraelectric phase[5,6] (no dipole) or an anti-ferroelectric phase[7,8] (antiparallel dipoles). Thus, in order to have a large ΔT near room temperature, the phase transition temperature should be close to room temperature.

However, the ΔT in bulk ceramics is always too low to be utilized in practical applications because the ECE in bulk ceramics is limited by the low breakdown strength. In 2006, Mischenko et al. reported an outstanding ECE (ΔT = 12 K under 480 kV/cm) in a 350 nm thick $PbZr_{0.95}Ti_{0.05}O_3$ film.[9] After that, many promising electrocaloric materials in the form of thin film were reported.[10-12] However, the heat extraction capacity is always lower in thin film than their ceramics counterparts.[13] Therefore, bulk electrocaloric materials are still being searched and studied.

So far, most electrocaloric ceramics are lead-containing. Their replacement by lead-free electrocaloric ceramics with comparable properties is necessary due to the concern of Pb toxicity. $(Bi_{1/2}Na_{1/2})TiO_3$ (BNT) has very complex phase transitions from rhombohedral to tetragonal and from tetragonal to cubic at around 300 and 540 ^oC, respectively.[14] The thermal

depoling process is found to occur at approximately 190 ºC in pure BNT.[15] Such a high depolarization temperature (T_d) makes pure BNT inferior in its room temperature ECE. Many dopants have been utilized to lower T_d of pure BNT. Bai et al. reported a $\Delta T = 0.19$ K around 100 ºC in $BaTiO_3$ doped BNT.[16] After that, $SrTiO_3$,[17] $KNbO_3$,[18] $(Ba,Sr)TiO_3$,[19] $(Bi,K)TiO_3$[20] were all chosen to obtain good ECE near room temperature.

In addition to ΔT, electrocaloric materials have also been evaluated using other figures of merit. T_{max}, at which the maximum ΔT appears, indicates the working temperature of an electrocaloric material. ΔS, the entropy change, represents the ECE under isothermal conditions. $\Delta T/\Delta E$, the electrocaloric responsivity, is used to quantify the ECE efficiency. Finally, T_{span} refers to the temperature range in which a large ΔT can be maintained in electrocaloric materials and is defined as the temperature span over which ΔT is greater than 90% of the maximum ΔT.[12]

Recently, our group reported giant large-signal piezoelectric coefficients (d_{33}*) in two $[Bi_{1/2}(Na,K)_{1/2}]TiO_3$-based ceramics, $\{[Bi_{1/2}(Na_{0.84}K_{0.16})_{1/2}]_{0.96}Sr_{0.04}\}(Ti_{0.975}Nb_{0.025})O_3$ and $[Bi_{1/2}(Na_{0.8}K_{0.2})_{1/2}](Ti_{0.985}Ta_{0.015})O_3$.[21,22] In this study, we used the indirect measurement to characterize the electrocaloric effect in both ceramics to demonstrate their potential multifunctional properties and to explore the mechanisms for ECE.

II. Experimental Procedure

Polycrystalline ceramics $\{[Bi_{1/2}(Na_{0.84}K_{0.16})_{1/2}]_{0.96}Sr_{0.04}\}(Ti_{0.975}Nb_{0.025})O_3$ (BNKT-2.5Nb) and $[Bi_{1/2}(Na_{0.8}K_{0.2})_{1/2}](Ti_{0.985}Ta_{0.015})O_3$ (BNKT-1.5Ta) were fabricated using the solid state reaction method. The raw materials of Na_2CO_3 (≥99.9 wt%), K_2CO_3 (≥99.0 wt%), Bi_2O_3 (≥99.9 wt%), TiO_2 (≥99.98 wt%), $SrCO_3$ (≥99.99 wt%), Nb_2O_5 (≥99.99 wt%) and Ta_2O_5 (≥99.99 wt%) were mixed in ethanol according to stoichiometry and milled in a vibratory mill for 6 or 7 hours. After

drying, the mixture for BNKT-2.5Nb was calcined twice at 850 ^{o}C for 3 hours and then sintered at 1175 ^{o}C for 3 hours. The mixture for BNKT-1.5Ta was calcined once at 850 ^{o}C for 3 hours and then sintered at 1150 ^{o}C for 3 hours.

The phase purity and crystal structure of the as-sintered ceramics were analyzed with X-ray diffraction (Model D500, Siemens, Germany). The temperature dependent heat capacity of the unpoled ceramics was determined by differential scanning calorimetry (DSC, model Q2000, TA Instrument) at a heating rate of 10 ^{o}C min^{-1}. The density of the ceramics was measured using the Archimedes Method.

Conventional and *in situ* transmission electron microscopy (TEM, FEI Tecnai G2-F20) was employed to reveal the domain structure of virgin state, and states exposed to electric field. For these observations, the as-sintered pellets were mechanically ground and polished to 120 μm. Disks of 3 mm in diameter were ultrasonically cut and the center portion was thinned to 10 μm by mechanical dimpling. Then, the BNKT-2.5Nb and BNKT-1.5Ta samples were annealed at 250 ^{o}C and 300 ^{o}C respectively for 0.5 hour to remove the residual stresses, followed by Ar-ion milling to the point of electron transparency. The details of the special configuration for *in situ* TEM have been outlined in our earlier publication.[23]

For electrical properties measurements, silver paste (Dupont 6160) was fired on both sides of the polished ceramics at 850 ^{o}C for 6 min to serve as electrodes. The longitudinal strain developed under the electric field in the form of a triangular wave of 0.1 Hz was monitored by MTI-2000 Fotonic Sensor (MTI Instruments Inc). The temperature-dependent dielectric constant and loss tangent were measured at frequencies of 120 Hz, 1 kHz and 10 kHz at a heating rate of 4 ^{o}C/min using an LCZ meter (3330; Keithley, Cleveland, OH). The polarization hysteresis (P-E)

loops were recorded by a standardized ferroelectric test system (RT-66A, Radiant Technologies) at 4 Hz at different temperatures.

III. Results

The room temperature X-ray diffraction patterns of BNKT-2.5Nb and BNKT-1.5Ta as-sintered ceramics are shown in Fig. 1. Both compositions form pure perovskite with a pseudo-cubic symmetry at room temperature. In both patterns, $(002)_{pc}$ diffraction peak at ~46.3° shows a very weak shoulder (inset of Fig. 1). The difference is that this shoulder is slightly more pronounced in BNKT-1.5Ta.

The bright field TEM images along the [112] zone axis of representative grains in BNKT-2.5Nb and BNKT-1.5Ta are shown in Fig. 2(a) and (b), respectively. The grains in both ceramics are mostly occupied by nanometer-sized domains. Superlattice diffraction spots in selected area electron diffraction (SAED) patterns are able to reveal the subtle deviation of crystal symmetry from the ideal cubic perovskite structure.[24]

In the insets of Fig. 2, [112] zone axis SAED of BNKT-2.5Nb and BNKT-1.5Ta are displayed. It is evident that two sets of superlattice spots, ½{*ooo*}-type marked by bright circles and ½{*ooe*}-type marked by bright arrows (*o* and *e* stand for odd and even Miller indices, respectively) appear in both compositions. According to our previous study on BNT-based ceramics,[25] BNKT-2.5Nb and BNKT-1.5Ta are mainly mixed rhombohedral *R3c* and tetragonal *P4bm* phases, both of which are in the forms of nanometer-sized domains. Notice that, ½{*ooe*} superlattice spots are more discrete than ½{*ooo*} in BNKT-1.5Ta; but in BNKT-2.5Nb, ½{*ooe*} spots are equally diffuse as ½{*ooo*} in some grains or more diffuse than ½{*ooo*} in the rest.

The electro-strains in BNKT-2.5Nb and BNKT-1.5Ta ceramics under bipolar field are displayed in Fig. 3. Highly asymmetric sprout-shaped strain loops are observable in both

samples. Asymmetry is also seen in the corresponding polarization loops (not shown). Defect dipoles are speculated to be responsible for the observed asymmetry.[22] Giant strains, 0.70% in BNKT-2.5Nb and 0.59% in BNKT-1.5Ta, are developed at positive peak field (50 kV/cm). These electro-strains are consistent with the range of measured values in our previous publications.[21,22] The giant strain in BNT-based ceramics is ascribed to the reversible field induced phase transition,[21,26] taking place in the ergodic relaxor which we believe to be the "relaxor ferrielectric" phase.[27]

The most intriguing feature of our BNKT-based ceramics is their outstanding large-signal piezoelectric coefficients (d_{33}*), 1400 pm V^{-1} in BNKT-2.5Nb and 1180 pm V^{-1} in BNKT-1.5Ta. In BNT-based ceramics, large d_{33}* can be realized around depolarization temperature.[28,29] In our materials, giant room temperature d_{33}* indicates that their T_d are very close to room temperature. In order to confirm this, we performed dielectric measurement on poled samples. Since our materials are mainly ergodic at room temperature, any ambient temperature poling is futile.[30] Instead we have to pole them at lower temperatures in their non-ergodic phase region. The dielectric constant and loss tangent data from -40 ^oC to 150 ^oC of both samples which are pre-poled at -40 ^oC are shown in Fig. 4(a) and (b). There is an obvious hump in the tanδ curve in both BNKT-2.5Nb (16 ^oC) and BNKT-1.5Ta (12 ^oC), which is defined as the depolarization temperature.[31] The slightly higher T_d in BNKT-2.5Nb probably accounts for its larger electro-strain at room temperature than BNKT-1.5Ta.

In order to quantify the electrocaloric effect by the indirect method, we measured P-E loops every 5 ^oC in the temperature range from 105 ^oC to 15 ^oC on cooling to minimize the reduction in polarization due to fatigue, given that the polarization degradation with cycling is indeed nontrivial in both BNKT-2.5Nb and BNKT-1.5Ta.[21,22] Mathematically, ECE calculations are not

perfectly reliable at both ends of the measuring temperature range. Therefore we just show our results between 100 ºC and 20 ºC. We can clearly see the pinched hysteresis loops instead of typical ferroelectric loops over the whole range from 100 ºC to 20 ºC in both ceramics (Fig. 5(a) and (c)), which are the signatures of reversible phase transitions between "relaxor ferrielectric" and ferroelectric under electric field. As samples are cooled down, hysteresis loop gradually becomes normal, reflecting the fact that ferroelectric phase becomes more stable at lower temperatures. We also measured the P-E loops at low temperature in BNKT-2.5Nb and BNKT-1.5Ta, with results displayed in Fig. 5 (b) and (d), respectively. BNKT-2.5Nb displays a typical ferroelectric loop at -10 ºC while BNKT-1.5Ta retains the pinched hysteresis loops at -30 ºC.

Based on Maxwell relations $(\partial P/\partial T)_E = (\partial S/\partial E)_T$, the reversible entropy change (ΔS) and temperature change (ΔT) are given by,

$$\Delta S = -\frac{1}{\rho}\int_{E_1}^{E_2}\left(\frac{\partial P}{\partial T}\right)_E dE \quad (1)$$

$$\Delta T = -\frac{1}{\rho}\int_{E_1}^{E_2}\frac{T}{C}\left(\frac{\partial P}{\partial T}\right)_E dE \quad (2)$$

where C is heat capacity and ρ is the material's density. The temperature dependence of polarization under various fields are extracted from the upper branches (E > 0) of P-E loops and values of $(\partial P/\partial T)$ are derived from sixth-order polynomial fit to *P(T)* data (Fig. 6). The temperature dependent heat capacity (in the range of 550 ~ 630 $J \cdot kg^{-1} \cdot K^{-1}$) measured by DSC in both ceramics is used for the calculation. The density is measured to be 5.44 g cm^{-3} and 5.48 g cm^{-3} for BNKT-2.5Nb and BNKT-1.5Ta, respectively.

ΔS and ΔT in BNKT-2.5Nb and BNKT-1.5Ta under various fields between 20 ºC and 100 ºC are shown in Fig. 6 (c), (d) and (g), (h) respectively. The figures of merit relating to the ECE in both ceramics are summarized in Table 1, together with some other electrocaloric materials' for

comparison. BNKT-2.5Nb has maximum ΔT = 1.85 K and ΔS = 2.83 $JKg^{-1}K^{-1}$ at 32 ^{o}C, implying that it can be potentially used as good electrocaloric ceramics operated around room temperature. More strikingly, $\Delta T/\Delta E$ reaches 0.37 ($10^{-6}KmV^{-1}$) in BNKT-2.5Nb, which is one of the highest among not only BNT-based, but even all lead-free electrocaloric ceramics studied so far. Compared to BNKT-2.5Nb, BNKT-1.5Ta is overshadowed in all figures of merit except for T_{span}. In BNKT-1.5Ta, T_{span} is as large as 55 K, much greater than 15 K in BNKT-2.5Nb. This means that BNT-1.5 Ta has a much broader working temperature range than BNKT-2.5Nb.

IV. Discussion

(1-x) $(Bi_{1/2}Na_{1/2})TiO_3$-x$(Bi_{1/2}K_{1/2})TiO_3$ forms a broad morphotropic phase boundary (MPB) in the range of x=0.16-0.20.[36] Our compositions lie within this region. However, the depolarization temperature at MPB is well above room temperature,[37] which is not ideal for room temperature electrocaloric materials given the fact that the maximum ΔT always appears around T_d. Nb and Sr or Ta dopants have the capability to lower T_d in BNT-based ceramics.[38] As T_d is being shifted toward room temperature, the increased structural instability makes the field-induced phase transition between *P4bm* ferrielectric phase and *R3c* ferroelectric phase easier at room temperature. As a result, large ΔT and giant electro-strain will be obtained around room temperature. According to our previous study,[21,22] BNKT-2.5Nb displays larger electro-strain than either BNT-2.0Nb or BNT-3.0Nb; BNKT-1.5Ta has higher electro-strain than BNT-1.0Ta and BNT-2.0Ta. It is likely that BNKT-2.5Nb and BNKT-1.5Ta have larger ΔT around room temperature than other samples with different doping amounts. Similar to other BNT-based ceramics, BNKT-2.5Nb and BNKT-1.5Ta have three phases coexisting around T_d (*R3c* and *P4bm* polar nano-regions (PNRs) embedded in $Pm\bar{3}m$ cubic matrix[39,40]). As stated previously,

ECE is triggered by the electric field which induces ferroelectric phase out of relaxor, paraelectric or anti-ferroelectric phase. In our materials, *R3c* and *P4bm* are both in the form of nanometer-sized domains, i.e., one is relaxor ferroelectric while the other is "relaxor ferrielectric". The ferrielctric *P4bm* is an anti-ferroelectrics with uncompensated dipole moments. The $Pm\bar{3}m$ cubic matrix is paraelectric. Thus there could be all three types of phase transitions in our materials. It is believed that the combination of mechanisms benefits electrocaloric and electromechanical responses simultaneously.[41]

In order to verify the mechanism of large electrocaloric response, especially in BNKT-2.5Nb, we conduct *in situ* TEM study (Fig. 7). At virgin state (Fig. 7(a)), the grain is occupied with nanometer-sized domains. When an electric field is applied along the marked direction (Fig. 7(b)), nanometer-sized domains are transformed to large lamellar domains in most part of the grain. Correspondingly, in the inset of Fig. 7(a), two sets of superlattice diffraction spots, ½{*ooe*} representing *P4bm* "relaxor ferrielectric" phase and ½{*ooo*} representing *R3c* relaxor ferroelectric phase, can be unambiguously seen in SAED at virgin state. However, when the sample is exposed to electric field, only one type of superlattice diffraction spots, 1/2{*ooo*}, remains visible in the electron diffraction pattern, indicating that only *R3c* phase remains. So, electric field is able to transform the mixed phases, including *R3c* and *P4bm* phases with nanometer-sized domains and the $Pm\bar{3}m$ cubic phase which is hard to detect through SAED, into *R3c* phase with large lamellar domains. The real temperature of the TEM specimen is slightly higher than room temperature due to the heating effect of electron beam, so the *in situ* TEM experiment actually reveals the microstructural change under electric field around the maximum ΔT. Thus, our *in situ* TEM result demonstrates the combination of mechanisms which contributes to the good ECE in BNKT-2.5Nb.

The frequency dispersion in dielectric constant (Fig. 4) in both BNKT-2.5Nb and BNKT-1.5Ta corroborates with their relaxor nature. In the prototype relaxor, $Pb(Mg_{1/3}Nb_{2/3})O_3$-$xPbTiO_3$, $Pm\bar{3}m \leftrightarrow R3m$ phase transition evolves from first-order in pure PMN to second-order as PT doping increases.[42] Similarly, our materials, in which BKT are doped into BNT, likely have a second-order $P4bm \leftrightarrow R3c$ transition.[43] Moreover, in PMN-based relaxor, there exists a critical applied field below which the phase transition stays first-order and above which it tends to be second-order.[44] In Fig. 6(a) and (e), the order parameter (polarization) shows no sudden drop with temperature even under zero field. Thus, the phase transition in our materials are closer to second order in which the energy barrier between *R3c* and *P4bm* is quite low and easy for the electric field to overcome. As a result, the low energy barrier enables electric field to stabilize ferroelectric order readily, which makes the maximum ΔT shift towards high temperature with increasing field and finally appear at temperature above T_d.[45]

Compared to BNKT-2.5Nb, BNKT-1.5Ta has a much broader T_{span} but lower ΔT. This is consistent with some earlier works which suggest that temperature dependence of ΔT can be reduced at the cost of ΔT's magnitude.[46] However, as discussed in last paragraph, phase transitions in both BNKT-2.5Nb and BNKT-1.5Ta are quite continuous. Therefore, we cannot use transition order to differentiate their electrocaloric properties. A closer examination of Fig. 6(h) indicates that under 10 kV/cm, one single peak exists at 29.5 ^oC. As the field is increased, a second peak around 70 ^oC starts to emerge. Under 50 kV/cm, two peaks are unambiguously visible and somehow overlapping, making the T_{span} much broader. This can be better seen in the T_{span} vs. E plot for both BNKT-2.5Nb and BNKT-1.5Ta shown in Fig. 8. Under 10 kV/cm, the T_{span} values are almost equal in the two ceramics. T_{span} increases with the applied field in BNKT-1.5Ta but keeps nearly field-independent for BNKT-2.5Nb. This distinction proves that the

broader T_{span} in BNKT-1.5Ta is attributed to the extra peak emerging under higher applied fields (>10 kV/cm). Interestingly, the second peak under 50 kV/cm is even slightly higher than the first one. Therefore, the maximum ΔT in BNKT-1.5Ta appears at 70 ^{o}C instead of the temperature around T_d, like BNKT-2.5Nb.

This "dual peaks" phenomenon is not rare in relaxors and was explained by the alignment of polar nano-regions (PNRs) under electric field.[4,47] In order to verify its validity in our materials, the polarization current density (J) vs electric field (E) curves of BNKT-2.5Nb and BNKT-1.5Ta are determined by taking the derivative of the polarization with respect to time, i.e., *dp(t)/dt* (Fig. 9). For each test temperature between 20 ^{o}C and 100 ^{o}C, there are four anomalies within one full cycle, two J_1 and two J_2. J_1 corresponds to the forward phase transition while J_2 represents the backward process.[48] Heated up from the vicinity of T_d (20 ^{o}C), the forward phase transition tends to become harder, that is, E_{J1} (the electric field at J_1) is supposed to increase.[49] In BNKT-2.5Nb, E_{J1} increases linearly between 20 ^{o}C and 50 ^{o}C. After 50 ^{o}C, E_{J1} continues to increase, but the peak for J_1 anomaly has exceeded our applied field, so we simply do not show the data for the higher temperature range (Fig. 9(c)). However, in BNKT-1.5Ta, E_{J1} increases before 40 ^{o}C but drops drastically between 40 ^{o}C and 70 ^{o}C. After 70 ^{o}C, E_{J1} stays nearly unchanged (Fig. 10(f)). We speculate that J_1 represents the *P4bm*→*R3c* phase transition for the whole temperature range in BNKT-2.5Nb, but only for the temperature lower than 40 ^{o}C in BNKT-1.5Ta; Above 40 ^{o}C, J_1 in BNKT-1.5Ta is more likely corresponding to the alignment of *P4bm* PNRs since the coalescence of nanodomains tends to get easier at higher temperature.[50] This speculation is in support to extra ECE peak at 70 ^{o}C for BNKT-1.5Ta.

The fundamental reason for the different ECEs in these two ceramics can be further discussed in terms of their base compositions. The base composition for BNKT-2.5Nb is 0.84BNT-0.16BKT

which is close to the *R3c*/*P4bm* MPB, while that for BNKT-1.5Ta is 0.8BNT-0.2BKT which is relatively closer to the *P4bm*/*P4mm* MPB. This is evidenced by the more pronounced shoulder of $(002)_{pc}$ diffraction peak in BNKT-1.5Ta than BNKT-2.5Nb (inset of Fig. 1). According to our previous study, the field-induced phase transition pathway depends upon the composition within the MPB.[51] So, the phase transition in BNKT-2.5Nb and BNKT-1.5Ta around room temperature, which leads to the giant electro-strain and decent ΔT (the first peak for BNKT-1.5Ta), can have different nature. This may also account for the difference in their d_{33}* and ΔT/ΔE. Apart from that, ferrielectric phase persists till lower temperatures in BNKT-1.5Ta than BNKT-2.5Nb (Fig. 5(b) and (d)) and the ½{*ooe*} supperlattice spots are more discrete than ½{*ooo*} in BNKT-1.5Ta (Fig. 2(b)). So, *P4bm* phase is more dominating in BNKT-1.5Ta, which probably gives rise to the *P4bm* nanodomains coalescence rather than phase transition around 70 ^{o}C.

Giant electro-strains and large electrocaloric responses are realized simultaneously in our materials, which makes them more promising, as multifunctional materials are always desired. Presumably, an even more attractive ΔT could be reached in BNKT-2.5Nb or BNKT-1.5Ta thin films due to much higher dielectric breakdown strength. When the films are confined by the substrate, giant electro-strains will likely generate large internal stresses, which in turn will affect the electrocaloric effect.[52,53] Thus, BNKT-2.5Nb and BNKT-1.5Ta can be further explored as multifunctional thin film materials in which properties could be mutually tuned.

V. Conclusions

The electrocaloric effect in both BNKT-2.5Nb and BNKT-1.5Ta ceramics, which are found to display giant electro-strains and large-signal piezoelectric coefficients, is evaluated indirectly. BNKT-2.5Nb displays a large ΔT = 1.85 K, ΔS = 2.83 $Jkg^{-1}K^{-1}$, and an excellent ΔT/ΔE = 0.37

($10^{-6}KmV^{-1}$) near room temperature (32 ^{o}C). BNKT-1.5Ta, on the other hand, exhibits a huge T_{span} of ~55 K. The good electrocaloric properties are attributed to the unique microstructures these ceramics have: nanodomains of a "relaxor ferrielectric" *P4bm* phase and a relaxor ferroelectric *R3c* phase, and a non-polar cubic phase. When combined with their giant electro-strains, both BNKT-2.5Nb and BNKT-1.5Ta ceramics are good candidates for active elements in multifunctional devices.

Reference

[1]. M. Valant, "Electrocaloric Materials for Future Solid-State Refrigeration Technologies," *Prog. Mater. Sci.*, **57**, 980-1009 (2012).

[2]. J. F. Scott, "Electrocaloric Materials," *Annu. Rev. Mater. Res.*, **41**, 229-240 (2011).

3. J. Hagberg, A. Uusimäki, and H. Jantunen. "Electrocaloric Characteristics in Reactive Sintered 0.87 Pb ($Mg_{1/3}Nb_{2/3}$)O_3-0.13 $PbTiO_3$," *Appl. Phys. Lett.*, **92**. 132909 (2008).

[4]. J. Peräntie, H. N. Tailor, J. Hagberg, H. Jantunen, and Z. -G. Ye, "Electrocaloric Properties in Relaxor Ferroelectric $(1-x)Pb(Mg_{1/3}Nb_{2/3})O_3–xPbTiO_3$ system," *J. Appl. Phys.*, **114**, 174105 (2013).

5. X. Liu, T. Chen, Y. Wu, and X. Chen, "Enhanced Electrocaloric Effects in Spark Plasma-Sintered $Ba_{0.65}Sr_{0.35}TiO_3$-Based Ceramics at Room Temperature," *J. Am. Ceram Soc.*, **96**, 1021-1023 (2013).

6. X. S. Qian, H. J. Ye, Y. T. Zhang, H. Gu, X. Li, C. A. Randall, and Q. M. Zhang, “Giant Electrocaloric Response over a Broad Temperature Range in Modified BaTiO3 Ceramics,” *Adv. Funct. Mater.*, **24**, 1300-1305 (2014).

7. Y. Zhao, X. H. Hao, and Q. Zhang, “A Giant Electrocaloric Effect of a $Pb_{0.97}La_{0.02}(Zr_{0.75}Sn_{0.18}Ti_{0.07})O_3$ Antiferroelectric Thick Film at Room Temperature,” *J. Mater. Chem. C.*, **3**, 1694-1699 (2015).

8. X. H. Hao, Y, Zhao, and Q, Zhang, “Phase Structure Tuned Electrocaloric Effect and Pyroelectric Energy Harvesting Performance of $(Pb_{0.97}La_{0.02})(Zr,Sn,Ti)O_3$ Antiferroelectric Thick Films,” *J. Phys Chem. C.*, **119**, 18877-18885 (2015).

9. A. S. Mischenko, Q. Zhang, J. F. Scott, R. W. Whatmore, and N. D. Mathur, “Giant Electrocaloric Effect in Thin-Film $PbZr_{0.95}Ti_{0.05}O_3$,” *Science*, **311**, 1270-1271 (2006).

10. A. S. Mischenko, Q. Zhang, R. W. Whatmore, J. F. Scott, and N. D. Mathur, “Giant Electrocaloric Effect in the Thin Film Relaxor Ferroelectric 0.9 $PbMg_{1/3}Nb_{2/3}O_3$-0.1 $PbTiO_3$ near Room Temperature,” *Appl. Phys. Lett.*, **89**, 242912 (2006).

11. T. M. Correia, S. Kar-Narayan, J. S. Young, J. F. Scott, N. D. Mathur, R. W. Whatmore, and Q. Zhang, “PST Thin Films for Electrocaloric coolers,” *J. Phys. D. Appl. Phys.*, **44**, 165407 (2011).

12. B. L. Peng, H. Q. Fan, and Q. Zhang, "A Giant Electrocaloric Effect in Nanoscale Antiferroelectric and Ferroelectric Phases Coexisting in a Relaxor $Pb_{0.8}Ba_{0.2}ZrO_3$ Thin Film at Room Temperature." *Adv. Funct. Mater.*, **23**, 2987-2992 (2013).

13. A. Chauhan, S. Patel, and R Vaish, “Elastocaloric Effect in Ferroelectric Ceramics,” *Appl. Phys. Lett.*, **106**, 172901 (2015).

14. J. A. Zvirgzds, P. P. Kapostin, J. V. Zvirgzds, and T. V. Kruzina, “X-ray Study of Phase Transitions in Ferroelectric $Na_{0.5}Bi_{0.5}TiO_3$,” *Ferroelectrics*, **40**, 75-77 (1982).

15. Y. Hiruma, H. Nagata, and T. Takenaka, “Thermal Depoling Process and Piezoelectric Properties of Bismuth Sodium Titanate Ceramics,” *J. Appl. Phys.*, **105**, 084112 (2009).

16. Y. Bai, G. P. Zheng, and S. Q. Shi, “Abnormal Electrocaloric Effect of $Na_{0.5}Bi_{0.5}TiO_3$–$BaTiO_3$ Lead-Free Ferroelectric Ceramics above Room Temperature,” *Mater. Res. Bull.*, **46**, 1866-1869 (2011).

17. W. Cao, W. Li, X. Dai, T. Zhang, J. Sheng, Y. Hou, and W. Fei, “Large Electrocaloric Response and High Energy-Storage Properties over a Broad Temperature Range in Lead-Free NBT-ST Ceramics,” *J. Eur. Ceram. Soc.*, **36**, 593-600 (2016).

18. X. Jiang, L. Luo, B. Wang, W. Li, and H. Chen, “Electrocaloric Effect Based on The Depolarization Transition in $(1-x)Bi_{0.5}Na_{0.5}TiO_3$–$xKNbO_3$ Lead-Free Ceramics,” *Ceram. Int.*, **40**, 2627-2634 (2014).

19. J. Tang, F. Wang, X. Zhao, H. Luo, L. Luo, and W. Shi, “Influence of the Composition-Induced Structure Evolution on the Electrocaloric Effect in $Bi_{0.5}Na_{0.5}TiO_3$-Based Solid Solution,” *Ceram. Int.*, **41,** 5888-5893 (2015).

20. W. Cao, W. Li, D. Xu, Y. Hou, W. Wang, and W. Fei, “Enhanced Electrocaloric Effect in Lead-Free NBT-Based Ceramics,” *Ceram. Int.*, **40**, 9273-9278 (2014).

21. X. Liu and X. Tan, “Giant Strains in Non-Textured $(Bi_{1/2}Na_{1/2})TiO_3$-Based Lead-Free Ceramics,” *Adv. Mater.*, **28**, 574-578 (2016).

22. X. Liu and X. Tan, “Giant Strain with Low Cycling Degradation in Ta-Doped $[Bi_{1/2}(Na_{0.8}K_{0.2})_{1/2}]TiO_3$ Lead-Free Ceramics,” *J. Appl. Phys.*, **120**, 034102 (2016).

23. X. Tan, H. He, and J. Shang, "*In situ* Transmission Electron Microscopy Studies of Electric-Field-Induced Phenomena in Ferroelectrics," *J. Mater. Res.*, **20**, 1641-1653 (2005).

24. D. I. Woodward and I. M. Reaney, "Electron Diffraction of Tilted Perovskites," *Acta. Crystallogr. B.*, **61**, 387-399 (2005).

25. C. Ma, X. Tan, E. Dui'kin, and M. Roth, "Domain Structure-Dielectric Property Relationship in Lead-Free $(1-x)(Bi_{1/2}Na_{1/2})TiO_3$- $xBaTiO_3$ Ceramics," *J. Appl. Phys.*, **108**, 104105 (2010).

26. W. Jo, T. Granzow, E. Aulbach, J. Rödel, and D. Damjanovic, "Origin of the Large Strain Response in $(K_{0.5}Na_{0.5})NbO_3$-Modified $(Bi_{0.5}Na_{0.5})TiO_3$–$BaTiO_3$ Lead-Free Piezoceramics," *J. Appl. Phys.*, **105**, 094102 (2009).

27. X. Tan, C. Ma, J. Frederick, S. Beckman, and K.G. Webber, "The Antiferroelectric↔ Ferroelectric Phase Transition in Lead-Containing and Lead-Free Perovskite Ceramics," *J. Am. Ceram Soc.*, **94**, 4091-4107 (2011).

28. K. Seifert, W. Jo, and J. Rödel, "Temperature-Insensitive Large Strain of $(Bi_{1/2}Na_{1/2})TiO_3$–$(Bi_{1/2}K_{1/2})TiO_3$–$(K_{0.5}Na_{0.5})NbO_3$ Lead-Free Piezoceramics," *J. Am. Ceram Soc.*, **93**, 1392-1396 (2010).

29. S. Zhang, A. Kounga, E. Aulbach, and Y. Deng, "Temperature-Dependent Electrical Properties of 0.94 $Bi_{0.5}Na_{0.5}TiO_3$–0.06 $BaTiO_3$ Ceramics," *J. Am. Ceram Soc.*, **91**, 3950-3954 (2008).

30. X. Liu, H. Guo, and X. Tan, "Evolution of Structure and Electrical Properties with Lanthanum Content in $[(Bi_{1/2}Na_{1/2})_{0.95}Ba_{0.05}]_{1-x}La_xTiO_3$ Ceramics," *J. Eur. Ceram. Soc.*, **34**, 2997-3006 (2014).

31. Y. Hiruma, H. Nagata, and T. Takenaka, "Phase Diagrams and Electrical Properties of $(Bi_{1/2}Na_{1/2})TiO_3$-Based Solid Solutions," *J. Appl. Phys.*, **104**, 4106 (2008).

32. L. Luo, M. Dietze, C. Solterbeck, M. Es-souni, and H. Luo, “Orientation and Phase Transition Dependence of the Electrocaloric Effect in $0.71PbMg_{1/3}Nb_{2/3}O_3$-$0.29PbTiO_3$ Single Crystal,” *Appl. Phys. Lett.*, **101**, 062907 (2012).

33. Z. Luo, et al., “Enhanced Electrocaloric Effect in Lead-Free $BaTi_{1-x}Sn_xO_3$ Ceramics near Room Temperature,” *Appl. Phys. Lett.*, **105**, 102904 (2014).

34. J. Koruza, B. Rožič, G. Cordoyiannis, B. Malič, and Z. Kutnjak, “Large Electrocaloric Effect in Lead-Free $K_{0.5}Na_{0.5}NbO_3$-$SrTiO_3$ Ceramics,” *Appl. Phys. Lett.*, **106**, 202905 (2015).

35. Y. Bai, X. Han, and L. Qiao, “Optimized Electrocaloric Refrigeration Capacity in Lead-Free $(1-x)\ BaZr_{0.2}Ti_{0.8}O_3$-$xBa_{0.7}Ca_{0.3}TiO_3$ Ceramics,” *Appl. Phys. Lett.*, **102**, 252904 (2013).

36. A. Sasaki, T. Chiba, Y. Mamiya, and E. Otsuki, “Dielectric and Piezoelectric Properties of $(Bi_{0.5}Na_{0.5})TiO_3$–$(Bi_{0.5}K_{0.5})TiO_3$ Systems,” *Jpn. J. Appl. Phys.*, **38**, 5564 (1999).

37. K. Yoshii, Y. Hiruma, H. Nagata, and T. Takenaka, “Electrical Properties and Depolarization Temperature of $(Bi_{1/2}Na_{1/2})TiO_3$–$(Bi_{1/2}K_{1/2})TiO_3$ Lead-free Piezoelectric Ceramics,” *Jpn. J. Appl. Phys.*, **45**, 4493 (2006).

38. R. Malik, J. Kang, A. Hussain, C. Ahn, H. Han, and J. Lee, “High Strain in Lead-Free Nb-Doped $Bi_{1/2}(Na_{0.84}K_{0.16})_{1/2}TiO_3$–$SrTiO_3$ Incipient Piezoelectric Ceramics,” *Appl. Phys. Express.*, **7**, 061502 (2014).

39. W. Jo, S. Schaab, E. Sapper, L. Schmitt, H. Kleebe, A. Bell, and J. Rödel, “On the Phase Identity and its Thermal Evolution of Lead Free $(Bi_{1/2}Na_{1/2})TiO_3$-6 mol% $BaTiO_3$,” *J. Appl. Phys.*, **110**, 074106 (2011).

40. E. Aksel, J. Forrester, B. Kowalski, J. Jones, and P. Thomas, “Phase Transition Sequence in Sodium Bismuth Titanate Observed Using High-Resolution X-ray Diffraction,” *Appl. Phys. Lett.*, **99**, 222901 (2011).

41. B. Peng, et al., “High Dielectric Tunability, Electrostriction Strain and Electrocaloric Strength at a Tricritical Point of Tetragonal, Rhombohedral and Pseudocubic phases,” *J. Alloy. Compd.*, **646**, 597-602 (2015).

42. Z. -G. Ye, Y. Bing, J. Gao, and A. A. Bokov, “Development of Ferroelectric Order in Relaxor (1− x) Pb ($Mg_{1/3}Nb_{2/3}$)O_3–x $PbTiO_3$ ($0 \leq x \leq 0.15$),” *Phys. Rev. B.*, **67**, 104104 (2003).

43. W. Jo, J. Daniels, D. Damjanovic, W. Kleemann, and J. Rödel, “Two-Stage Processes of Electrically Induced-Ferroelectric to Relaxor Transition in 0.94 ($Bi_{1/2}Na_{1/2}$)TiO_3-0.06 $BaTiO_3$,” *Appl. Phys. Lett.*, **102**, 192903 (2013).

44. Z. Kutnjak, J. Petzelt, and R. Blinc, “The Giant Electromechanical Response in Ferroelectric Relaxors as a Critical Phenomenon,” *Nature*, **441**, 956-959 (2006).

45. X. Hao and J. Zhai, “Electric-Field Tunable Electrocaloric Effects from Phase Transition between Antiferroelectric and Ferroelectric Phase,” *Appl. Phys. Lett.*, **104**, 022902 (2014).

46. R. Chukka, J. Cheah, Z. Chen, P. Yang, S. Shannigrahi, J. Wang, and L. Chen, “Enhanced Cooling Capacities of Ferroelectric Materials at Morphotropic Phase Boundaries,” *Appl. Phys. Lett.*, **98**, 2902 (2011).

47. L. J. Dunne, M. Valant, A. Axelsson, G. Manos, and N. M. Alford, “Statistical Mechanical Lattice Model of the Dual-Peak Electrocaloric Effect in Ferroelectric Relaxors and the Role of Pressure,” *J. Phys. D. Appl. Phys.*, **44**, 375404 (2011).

48. H. Guo, X. Liu, F. Xue, L. Chen, W. Hong, and X. Tan, “Disrupting Long-Range Polar Order with an Electric Field,” *Phys. Rev. B.*, **93**. 174114 (2016).

49. G. Viola, R. Mckinnon, V. Koval, A. Adomkevicius, S. Dunn, and H. Yan, “Lithium-Induced Phase Transitions in Lead-Free $Bi_{0.5}Na_{0.5}TiO_3$ Based Ceramics,” *J. Phys. Chem. C.*, **118**. 8564-8570 (2014).

50. H. Guo, C. Ma, X. Liu, and X. Tan, “Electrical Poling Below Coercive Field for Large Piezoelectricity,” *Appl. Phys. Lett.*, **102**. 092902 (2013).

51. C. Ma, H. Guo, S. Beckman, and X. Tan, “Creation and Destruction of Morphotropic Phase Boundaries through Electrical Poling: A Case Study of Lead-Free ($Bi_{1/2}Na$ 1/2) TiO_3−$BaTiO_3$ Piezoelectrics,” *Phys. Rev. Lett.*, **109**, 107602 (2012).

52. G. Akcay, S. P. Alpay, J. V. Mantese, and G. A. Rossetti, “Magnitude of the Intrinsic Electrocaloric Effect in Ferroelectric Perovskite Thin Films at High Electric Fields,” *Appl. Phys. Lett.*, **90**, 2909 (2007).

53. S. Patel, A. Chauhan, and R. Vaish, “Mechanical Confinement for Tuning Ferroelectric Response in PMN-PT Single Crystal,” *J. Appl. Phys.*, **117**, 084102 (2015).

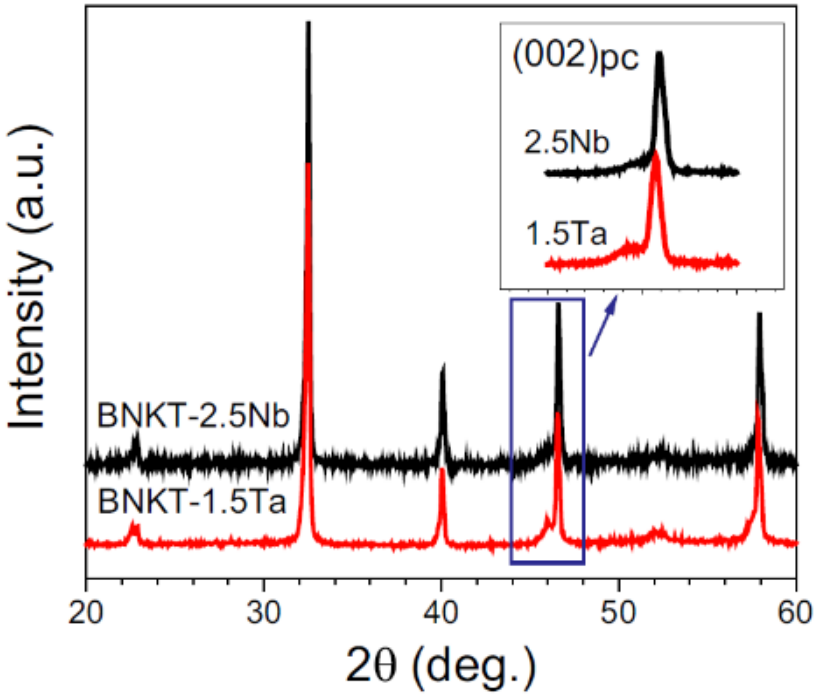

Fig. 1. X-ray diffraction patterns of as-sintered BNKT-2.5Nb and BNKT-1.5Ta polycrystalline ceramics. The inset shows the comparison of $(002)_{pc}$ diffraction peak between two ceramics.

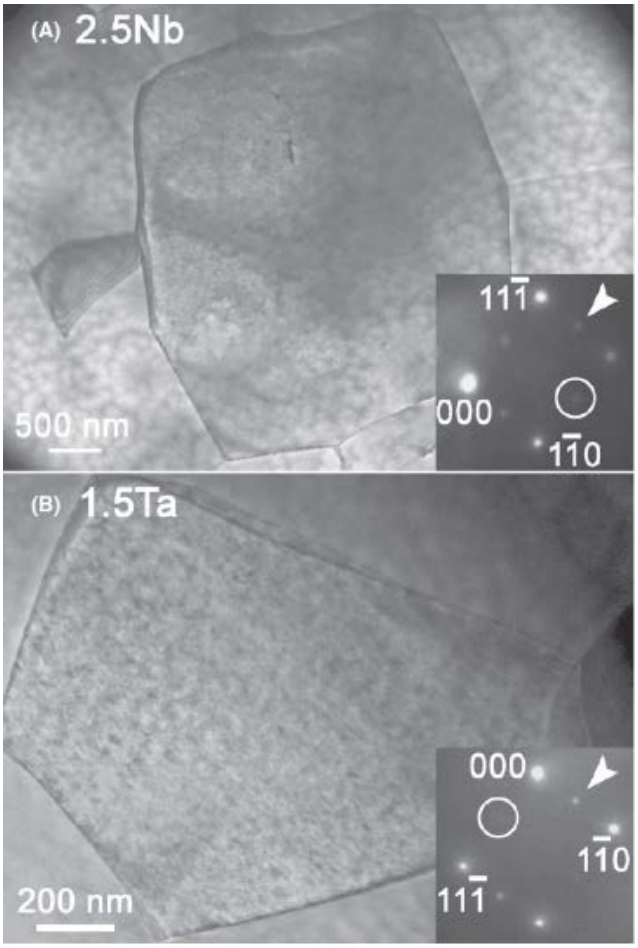

Fig. 2. TEM bright field micrographs of (a) BNKT-2.5Nb and (b) BNKT-1.5Ta examined along the [112] zone axis. The corresponding selected area electron diffraction patterns are shown as the insets. The ½{*ooo*}-type and the ½{*ooe*}-type superlattice spots are indicated by bright circles and arrows, respectively.

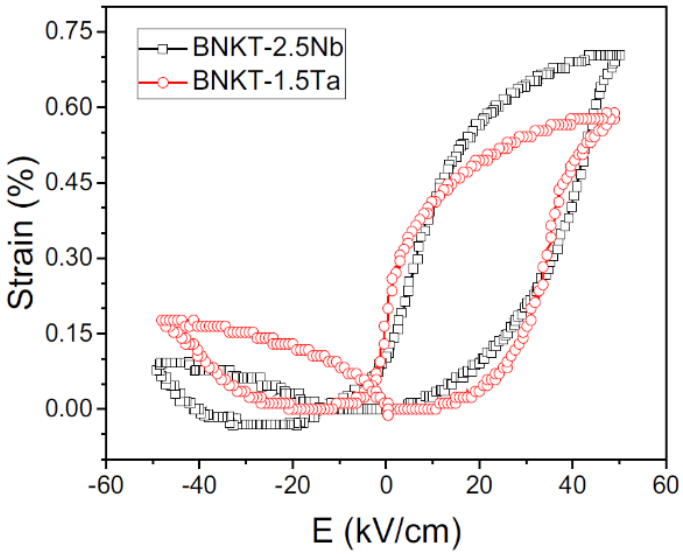

Fig. 3. Strain developed under bipolar electric fields of 50 kV/cm in BNKT-2.5Nb and BNKT-1.5Ta. Error bars are on the order of the size of symbols.

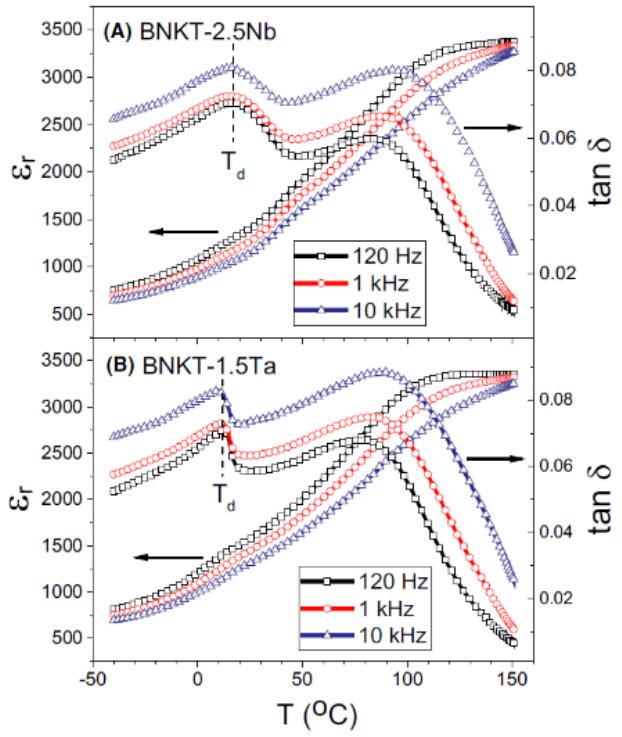

Fig. 4. Temperature dependent dielectric constant (ε_r) and loss tangent (tanδ) measured during heating on (a) BNKT-2.5Nb and (b) BNKT-1.5Ta, after the samples were poled with 50 kV/cm at -40 °C for 10 minutes. Error bars are on the order of the size of symbols.

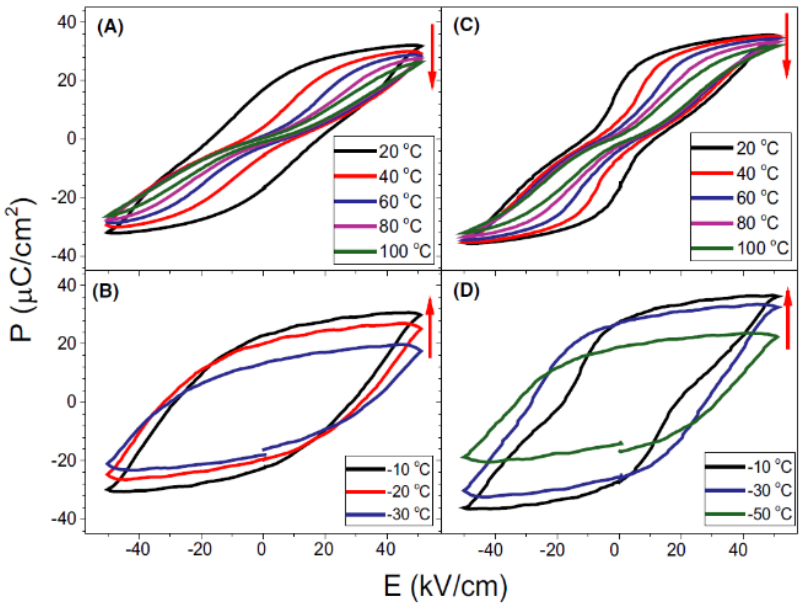

Fig. 5. Polarization developed under bipolar electric fields of 50 kV/cm at a series of temperatures in (a),(b) BNKT-2.5Nb and (c),(d) BNKT-1.5Ta.

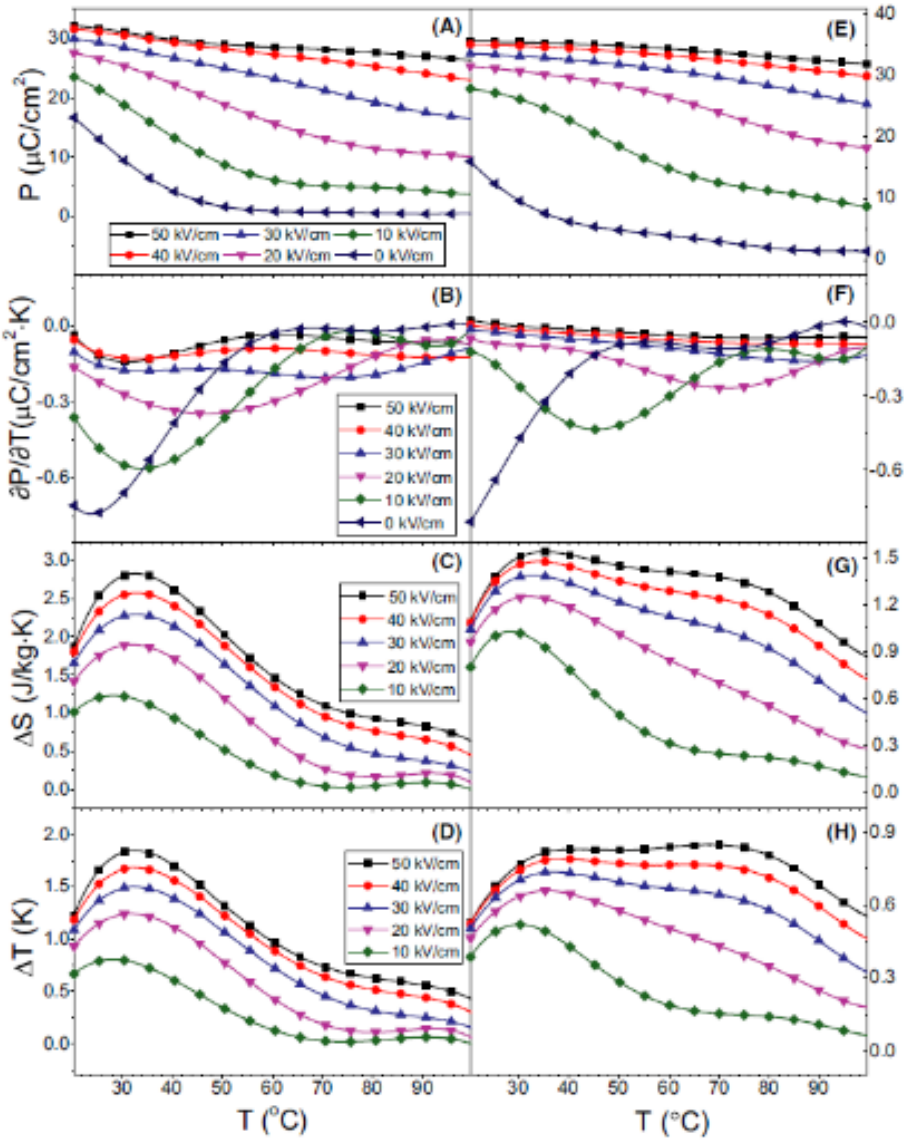

Fig. 6. Temperature dependence of (a),(e) polarization, (b),(f) pyroelectric coefficient, (c),(g) entropy change, (d),(h) temperature change in (a)-(d) BNKT-2.5Nb and (e)-(h) BNKT-1.5Ta under different fields. The red arrows point to the increased temperature.

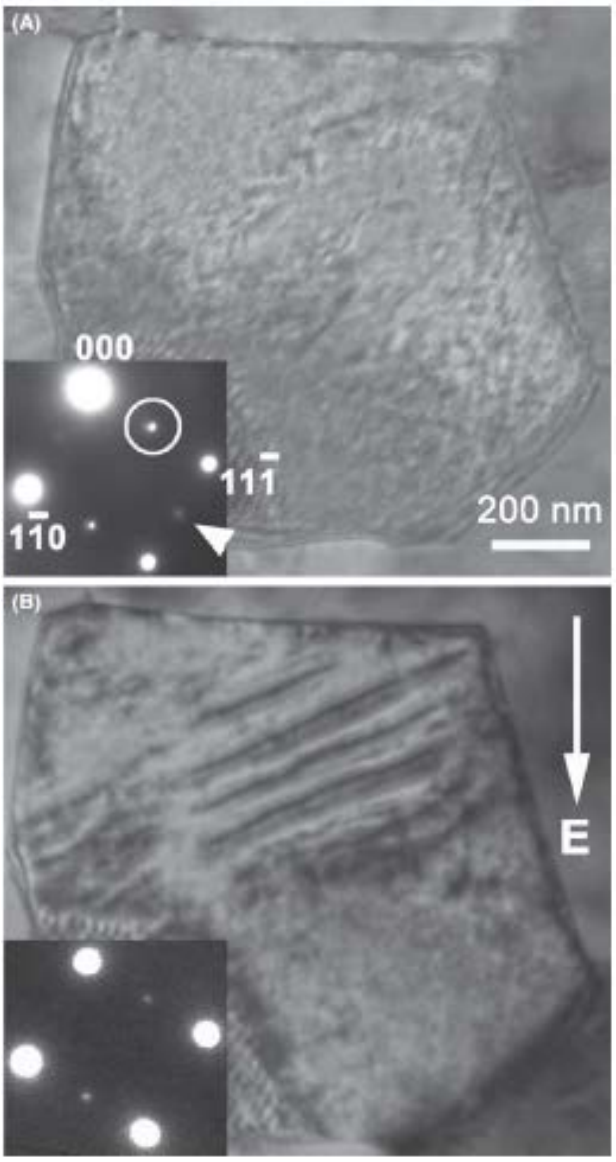

Fig. 7. *In situ* TEM of BNKT-2.5Nb along the [112] zone axis. (a) Domain morphology and selected area electron diffraction pattern at virgin state, (b) domain morphology and selected area electron diffraction pattern at the peak field (~50 kV/cm). The direction of the applied field is indicated by the bright arrow in (b). The bright circle and arrow in the diffraction pattern indicate the ½{*ooo*} and ½{*ooe*} superlattice diffraction spots, respectively.

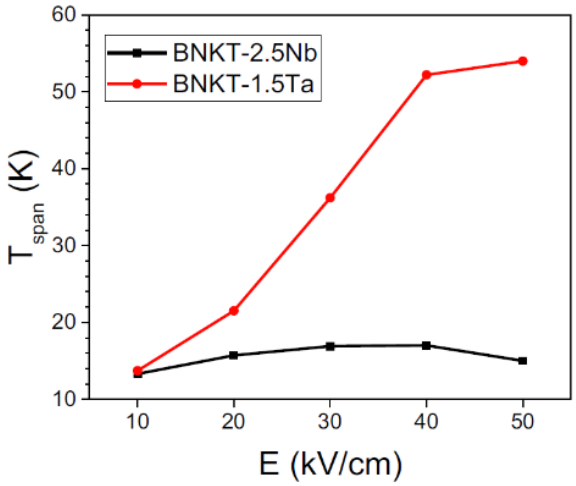

Fig. 8. Field-dependence of T_{span} in BNKT-2.5Nb and BNKT-1.5Ta, respectively.

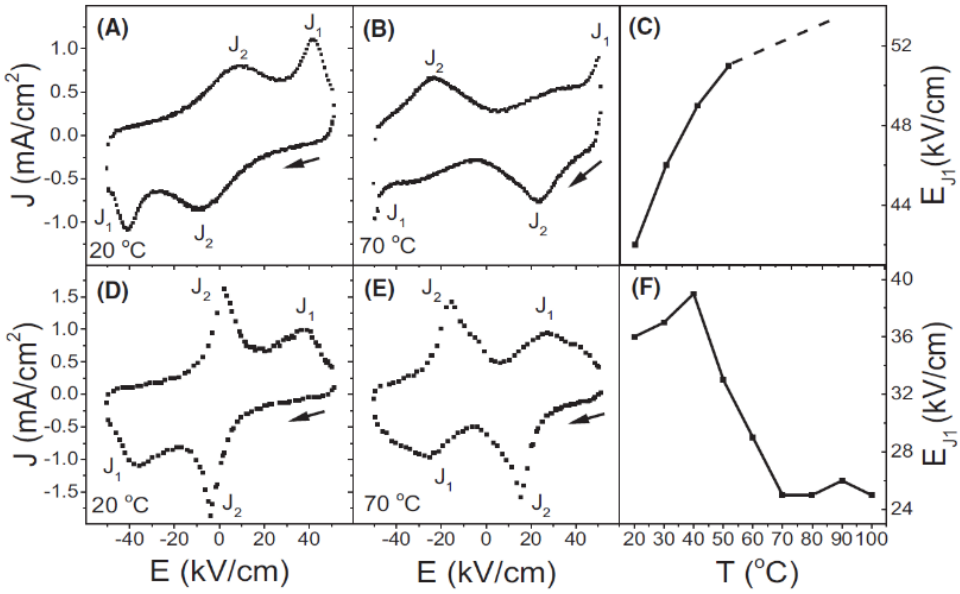

Fig. 9. Field-dependent current density in (a),(b) BNKT-2.5Nb and (d),(e) BNKT-1.5Ta at 20 ºC and 70 ºC, respectively; and temperature-dependence of E_{J1} in (c) BNKT-2.5Nb and (f) BNKT-1.5Ta.

Table 1. Figures of merit of selected electrocaloric materials.

Composition	Form	T_{max} (°C)	ΔT (K)	ΔE ($kVcm^{-1}$)	ΔS ($J \cdot kg^{-1} \cdot K^{-1}$)	ΔT/ΔE ($10^{-6} KmV^{-1}$)	T_{span} (K)	Reference
BNKT-2.5Nb	ceramics	32	1.85	50	2.83	0.37	~15	This work
BNKT-1.5Ta	ceramics	70	0.85	50	1.53	0.17	~55	This work
NBT-xST (x=0.25)	ceramics	60	1.64	60	2.52	0.33	~20	17
BNT-xKN (x=0.06)	ceramics	76	1.73	70	2.72	0.25	~25	18
0.94NBT-0.06BT	ceramics	100	1.50	50	2.20	0.30	~25	20
BZT (x=0.2)	ceramics	39	4.5	14.5	7.83	0.31	~30	6
$Pb_{80}Ba_{20}ZrO_3$	thin film	17	45.3	598	46.9	0.76		12
$PbZr_{0.95}Ti_{0.05}O_3$	thin film	222	12	480	8	0.25		9
0.71PMN-0.29PT	single crystal	171	2.3	50		0.46		32
0.9PMN-0.1PT	thin film	75	5	895		0.05		10
BSTM	ceramics	20	3.08	90	4.77	0.24		5
BTxSn (x = 0.105)	ceramics	28	0.61	20		0.31	~20	33
0.85KNN-0.15ST	ceramics	67	1.9	159	3.60	0.12		34
0.7BZT-0.3BCT	ceramics	60	0.3	20		0.15	~40	35